RSC Advances

ROYAL SOCIETY OF CHEMISTRY

www.rsc.org/advances

Journal Name

ARTICLE

Amino-functionalized metal-organic framework for adsorption and separation of dichloromethane and trichloromethane

Received 00th January 20xx,
Accepted 00th January 20xx

DOI: 10.1039/x0xx00000x

www.rsc.org/

Fengming Tian, Xinghua Zhang and Yunlin Chen*

Zinc-based metal organic framework MOF-5, and its amino-functionalized form IRMOF-3 were successfully synthesized, characterized, and evaluated for adsorption and separation of dichloromethane (DCM) and trichloromethane (TCM). Adsorption equilibria and kinetics of DCM and TCM on the two samples were measured at 298 K, 308 K, and 318 K. In spite of the reduced porosity of IRMOF-3, the adsorption capacity of DCM and TCM were improved up to 24.5 % and 27.4 % when compared with MOF-5. Therefore, the additional amino group in the MOF imparts extra adsorption capability on the MOF. The binary adsorption selectivity and diffusion selectivity of DCM and TCM are predicted via the Ideal Adsorbed Solution Theory (IAST) method. The adsorption selectivity and diffusion selectivity of DCM/TCM on the IRMOF-3 was about 5.62 and 3.88 at 298 K and 2.8 kPa, which were higher than those of MOF-5. The improved adsorption capacity and enhanced adsorption selectivity and diffusion selectivity over IRMOF-3 (with amino group) could be attributed to the improved interaction of DCM and TCM with the amino group on MOF.

1. Introduction

Metal-organic frameworks (MOFs), or porous coordination polymer (PCPs) constructed from inorganic secondary building units (SBUs) and bridging organic ligands[1-4] have attracted great attention because they can be applied in gas adsorption[5-7] and separation,[8] catalysis,[9, 10] and chemical sensing[11] due to their extra high surface area and pore volume as well as uniform and tunable openings. MOFs show an easy tunability for their structural modification including changing the linkers or imparting specific functional group, such as -NH_2, -OCH_3, -OH and so on.[12] Investigations into the application of amino functionalized MOFs in gas storage, separation and catalysis have been widely reported. Amino functionalized MOFs (NH_2-MIL-53(Al) or NH_2-MIL-101 (Al)) were used as dispersed phase in the fabrication of mixed matrix membranes, which indicating that amino group has enhanced the gas selectively adsorption properties of H_2/CH_4 and CO_2/CH_4.[13] MIL-125 and its amine-functionalized NH_2-MIL-125 were prepared and their adsorption and catalytic properties were characterized systematically.[14] Amine-modified Mg-MOF-74 membrane with higher H_2/CO_2 selectivity of 28 than as-synthesized MOF-74 with 10.5 since the modification with amine groups enhanced the strong adsorption of CO_2 molecules that reduces the permeance of CO_2.[15] Adsorption of indole was studied over UiO-66 and UiO-66-NH_2, and the results showed UiO-66-NH_2 has a significant 46% improvement of adsorption capacity over indole compared with pristine UiO-66 due to forming H-bonding between amino group and indole.[16] In our recent work, MOF-5 that consists of Zn_4O clusters linked by terephthalate acid and IRMOF-3 constructed with four Zn_4O clusters linked by 2-aminoterephthalic acid were selected as the adsorbents due to their similar structure to investigate the influence of amino group on the gas adsorption and separation property. In addition, there are numerous studies of IRMOF-3 have concentrated on catalysis[17-20] but rarely studied in gas adsorption. Recently, only one paper reported that IRMOF-3 was used as adsorbent for removal of dimethyl sulfide, ethyl mercaptan and hydrogen sulfide in fixed bed reactor at ambient temperature.[21]

Volatile organic compounds (VOCs) are among the most common air pollutants emitted from chemical, petrochemical and allied industries. Chlorinated volatile organic compounds (Cl-VOCs) is a subgroup of VOCs containing chlorine compounds, which have been widely used in the chemical industries including the manufacturing of herbicide, pesticide, paint, solvents, and pharmaceutical.[22] Dichloromethane (DCM) and trichloromethane (TCM) (as two of the representative Cl-VOCs) are included in the list of the 17 highly dangerous chemicals targeted in the emissions reduction effort of the US Environmental Protection Agency (EPA) due to their high toxicity and carcinogenic character. In addition, they contribute to global warming, the depletion of the ozone layer, and the formation of photochemical smog. Thus, the removal of DCM and TCM is a major environmental concern. Among the removal technologies of the pollutants emitted in air, adsorption is a well-established and effective technique for the removal and recovery of Cl-VOCs from polluted air. In our previous work,[23] we have investigated the adsorption and

Institute of Applied Micro-Nano Materials, School of Science, Beijing Jiaotong University, Beijing 100044, People's Republic of China. E-mail: ylchen@bjtu.edu.cn
† Electronic Supplementary Information (ESI) available. See DOI: 10.1039/x0xx00000x

separation of DCM and TCM on HKUST-1. The results showed that HKUST-1 consisting of two types of pores (large 9 Å cavities and small 5 Å tetrahedral pockets) has molecular sieve effect on adsorption and separation of DCM (3.3 Å) and TCM (6.5 Å) with high adsorption selectivity (3.04) and diffusivity selectivity (8.93) at 318 K and 2.8 kPa. To the best of the authors' knowledge, MOF-5 and IRMOF-3 have not been studied in details for DCM and TCM adsorption including adsorption equilibrium at different temperatures, isosteric heat of adsorption, and adsorption kinetics. In addition, the influence of amino group in IRMOF-3 on gas adsorption and separation has not been reported so far.

In this work, we have synthesized and characterized MOF-5 and IRMOF-3 and conducted a comprehensive investigation on the adsorption and diffusion properties of DCM and TCM. The equilibrium data were obtained at 298 K, 308 K, and 318 K with the pressure up to their saturated vapor pressure for DCM and TCM. The Langmuir isotherm model was employed to correlate the adsorption isotherms. The isosteric heats were calculated to evaluate the interactions between adsorbates and adsorbents. The diffusion coefficients of DCM and TCM within MOF-5 and IRMOF-3 were calculated on the basis of its adsorption kinetic data. In addition, the DCM/TCM vapor adsorption selectivity and kinetic selectivity on MOF-5 and IRMOF-3 were estimated using IAST method. Based on these results, we also systematically discussed the influence of amino group in MOFs on the gas adsorption and separation performance of DCM and TCM.

2. Experimental

2.1 Synthesis

Zinc nitrate hexahydrate ($Zn(NO_3)_2{\cdot}6H_2O$), 1,4-benzenedicarboxylic acid (H_2BDC), 2-Aminobenzene-1,4-dicarboxylic acid (NH_2-H_2BDC), N,N'-dimethylformamide (DMF) were of analytical reagent grade from commercial sources and used without further purification and modification.

MOF-5 crystals were synthesized following the reported procedures with a few modifications.[24] In a typical preparation, $Zn(NO_3)_2{\cdot}6H_2O$ (8.4 mmol) and H_2BDC (3.18 mmol) were dissolved in 60 mL of DMF and stirred for 20 min at room temperature. The solution was then transferred into Teflon-lined stainless steel autoclave and heated at 398 K for about 24 h. The resulting crystals were immersed in chloroform in a capped vial at 343 K for another 3 days. The MOF-5 crystals were heated at 423 K under vacuum overnight in order to remove present solvents, moisture, and other volatile components.

IRMOF-3 crystals were synthesized according to the procedure from literature with slight modifications.[25] In a typical preparation, $Zn(NO_3)_2{\cdot}6H_2O$ (7.5 mmol) and NH_2-H_2BDC (2.5 mmol) were dissolved in 60 mL DMF and stirred for 20 min at room temperature. The solution was transferred and sealed in a Teflon-lined autoclave, and kept at 373 K for 20 h. The resulting brown solid was collected and immersed in chloroform in a capped vial at 343 K for another 3 days. The IRMOF-3 crystals were heated at 423 K under vacuum overnight in order to remove present solvents, moisture, and other volatile components.

2.2 Characterization

X-ray diffraction (XRD) was carried out on a Rigaku D/Max-2500 X-ray diffractometer at 40 kV, 120 mA with a scan speed of 10°/min and a step size of 0.02° in 2 θ range from 5° to 20°, using Cu Kα radiation (wavelength λ=0.1543 nm). Optical Microscope (OM) studies were conducted with 6XB-PC microscope. Scanning electron microscopy (SEM) studies were conducted with a HITACHI S-4800 SEM (Japan) operating at an accelerating voltage of 10 kV and 10 μA after gold deposition. Nitrogen adsorption and desorption isotherms, Langmuir area and Brunauer-Emmet-Teller (BET) surface area of the samples were measured by Quadrasorb SI at liquid nitrogen temperature of 77 K. Prior to gas adsorption measurements, the samples were activated by heating at 423 K under a reduced pressure.

2.3 Measurements of adsorption isotherms of DCM and TCM

The adsorption isotherms of DCM and TCM (>99.9%, from Shanghai HPLC) on the MOFs were measured using a standard gravimetric method with Intelligent Gravimetric Analyser (IGA-003, HIDEN). The physicochemical properties of DCM and TCM are listed in ESI (Table S1†). The IGA-003 is equipped with an ultra-sensitive balance of resolution 0.2 mg mounted in the thermostated heat sink with high precision temperature control. About 60-70 mg samples was weighted for each run. Prior to the measurements, the sample in the vessel of the IGA-003 was vacuumed up to 3-5 Pa and outgassed at 423 K for 24 h to remove any residual guests, the adsorbed water, and gases. After that, isotherms of DCM and TCM on the sample were measured at 298, 308, and 318 K. The highest adsorption pressure was the saturated vapor pressures at the corresponding temperatures (see ESI, Table S1 †). The equilibrium and instantaneous uptakes of DCM and TCM on the sample can be calculated as follows:

$$Q_e = \frac{1000(W_e - W_a)}{W_a M}$$

$$Q_t = \frac{1000(W_t - W_a)}{W_a M}$$

where M (g/mol) is the molecular weight of DCM or TCM molecule; W_e (g) and W_t (g) are the amount of adsorbent at equilibrium and time t (min); W_a (g) is the initial weight of the sample; and Q_e (mmol/g) and Q_t (mmol/g) are the DCM or TCM amount adsorbed per gram of adsorbent at equilibrium and at time t (min), respectively. Kinetic data were collected at the same time when the isotherms were measured.

3. Results and Discussion

3.1 Characterization and physical properties of the MOFs

Structures of the as-synthesized MOF-5 and IRMOF-3 crystals were characterized by X-ray diffraction (XRD). MOF-5 consists of Zn_4O clusters and terephthalate acid (H_2BDC) linkers and

IRMOF-3 constructed with Zn_4O clusters linked by 2-aminobenzenedicarboxylate (NH_2-BDC), which forming extended three-dimensional cubic porous network as $Zn_4O(BDC)_3$ and $Zn_4O(NH_2BDC)_3$, respectively. As it can be seen in Fig. 1, all diffraction peaks in the XRD patterns of the two samples match well with the patterns calculated from their corresponding crystallographic data obtained from their single-crystal X-ray diffraction, respectively, indicating the formation of pure-phase MOF-5 and IRMOF-3. In addition, the XRD patterns of MOF-5 and IRMOF-3 synthesized in this work agreed well with those reported in published literatures on the MOF-5[26, 27] and IRMOF-3 crystals[17, 28]. IRMOF-3 (NH_2-MOF-5) which is comprised of Zn^{2+} clusters interconnected by the same 2-amiono benzenedicarboxylate ligand as in NH_2-MIL-125[14] is more stable against moisture than the isostructural MOF-5 (without the amino group in the ligand) because of the intramolecular hydrogen bonding between the aromatic amino hydrogen atom and a carboxylate oxygen atom in the structure.[29]

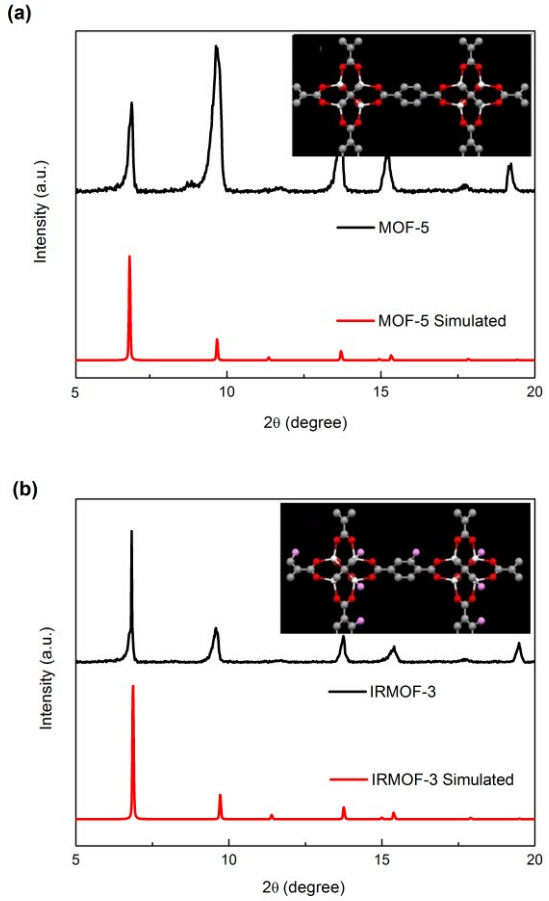

Fig.1 XRD patterns of the as-synthesized (a) MOF-5 and (b) IRMOF-3.

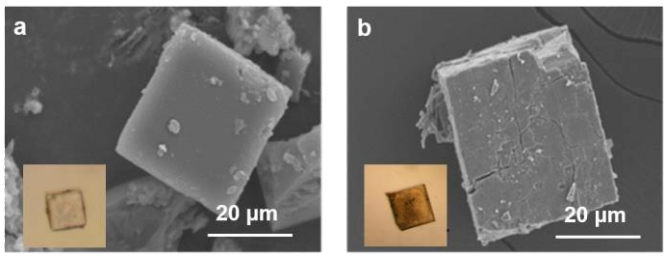

Fig.2 Optical Microscope (OM) images and scaning electron microscope (SEM) images of the as-synthesized (a) MOF-5 and (b) IRMOF-3 crystals.

OM images and SEM images were used to investigate the morphologies, crystallinity, and microstructures of the synthesized MOF-5 and IRMOF-3 crystals (shown in Fig. 2). The synthesized MOF-5 colorless crystal has a cubic morphology and uniform size of approximately 30 μm. The synthesized IRMOF-3 brown crystal has a cubic morphology and uniform size of approximately 35 μm. The well facetted crystals with uniform crystals size have clean and smooth surface. It is illustrated that our synthesized MOF-5 and IRMOF-3 crystals depict a perfect crystallization with high purity.

Pore textural properties for MOF-5 and IRMOF-3 were calculated from the nitrogen adsorption-desorption isotherms plotted in Fig. 3. Table 1 summarizes the pore textural properties for MOF-5 and IRMOF-3 including Langmuir specific surface area, BET specific surface area, maximum pore volume and median pore diameter calculated by HK method. The N_2 isotherms on MOF-5 and IRMOF-3 are of type I with an initial steep increase in the nitrogen uptake followed by a plateau at high pressures. The BET surface area, Langmuir surface area, and pore volume of MOF-5 is 1609.34 m^2/g and 2017.26 m^2/g and 1.39 cm^3/g, respectively. The pore size distribution curve

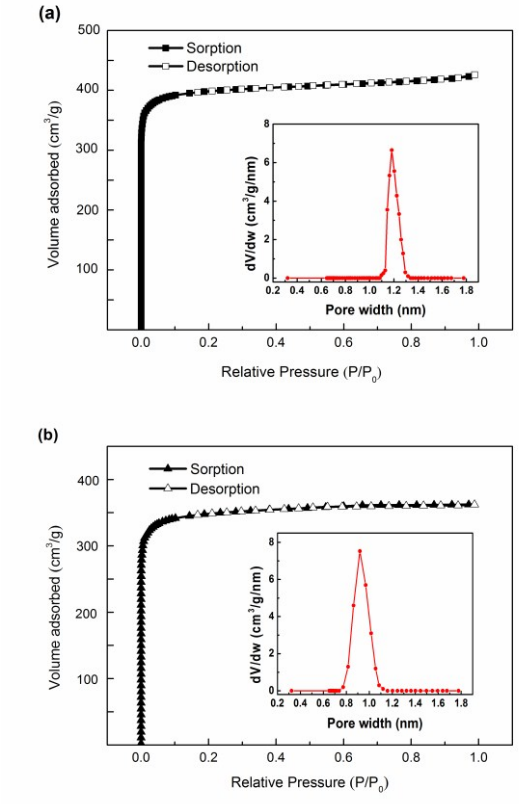

Fig.3 Nitrogen adsorption/desorption isotherm of (a) MOF-5 and (b) IRMOF-3 crystals at 77 K and their corresponding pore size distribution calculated by Horvath-Kawazoe (HK) method.

Table 1 Pore textural properties of MOF-5 and IRMOF-3 crystals

Adsorbent	$S_{Langmuir}$ ($m^2 \cdot g^{-1}$)	S_{BET} ($m^2 \cdot g^{-1}$)	A_{HK} (nm)	V_{pore} ($cm^3 \cdot g^{-1}$)
MOF-5	2017.26	1609.34	1.21	1.39
IRMOF-3	1740.51	1328.72	1.02	1.08

$S_{Langmuir}$: Langmuir specific surface area; S_{BET}: BET specific surface area; A_{HK}: pore aperture; V_{pore}: pore volume.

shows a monodisperse pore size with 1.02 nm in IRMOF-3, which is smaller than those in MOF-5 (1.21 nm) due to the presence of amino groups projecting into the pores. The BET surface area, Langmuir surface area, and pore volume of IRMOF-3 is 1328.72 m^2/g and 1740.51 m^2/g and 1.08 cm^3/g, respectively. Nitrogen physisorption measurements indicated that the IRMOF-3 has smaller pore size and pore volume than those of MOF-5, indicating that the amino group has reduced the pore size and pore volume. The uniform microporous structure of the synthesized MOF-5 and IRMOF-3 indicates the high crystallinity of the MOFs.

3.2 Adsorption Equilibrium

Fig. 4 shows separately the adsorption isotherms of DCM and TCM on the MOF-5 and IRMOF-3 with different temperatures at the pressure from vacuum to its saturated pressure. All the adsorption isotherms exhibit type-I isotherm with a sharp increase section followed by a plateau, suggesting strong interaction between the MOFs and Cl-VOCs. In Fig. 4a, it was observed that MOF-5 has the highest adsorption amount of 8.49 mmol/g for DCM at 298 K, which is much higher than that of activated carbon (1.88 mmol/g)[30] and that of dealuminated faujasite Y (DAY) zeolite at 298 K (3.18 mmol/g)[31]. In Fig. 4b, it is clearly visible that the maximum adsorption capacity of the MOF-5 for TCM is up to 6.14 mmol/g at 298 K, which is higher than that of activated carbon at 300.15 K (4.8 mmol/g)[32] and that of Na-$Y_{5.5}$ zeolite at 303 K (3 mmol/g)[33]. The higher adsorption capacity of DCM and TCM on MOF-5 is attributed to the much larger specific surface area of MOF-5 (BET of 2109.3 $m^2 \cdot g^{-1}$). In Fig. 4c, it was observed that IRMOF-3 has the adsorption amount of 10.57 mmol/g for DCM, which is higher than that of MOF-5 at 298 K. It is clearly visible that the maximum adsorption capacity of the IRMOF-3 for TCM is up to 7.82 mmol/g at 298 K (showed in Fig. 4d), which is also higher than that of MOF-5. The higher adsorption capacity of DCM and TCM on IRMOF-3 is attributed to amino group. Hence, this microporous MOF with amino group exhibits excellent adsorption behavior at trace concentration levels and may become one of the promising candidates for Cl-VOCs capture applications. It can be seen that the uptakes of Cl-VOCs on the MOF-5 and IRMOF-3 both decreased with temperature, and the lower the temperature was, the larger the Cl-VOCs uptake, which meant that the adsorption of DCM

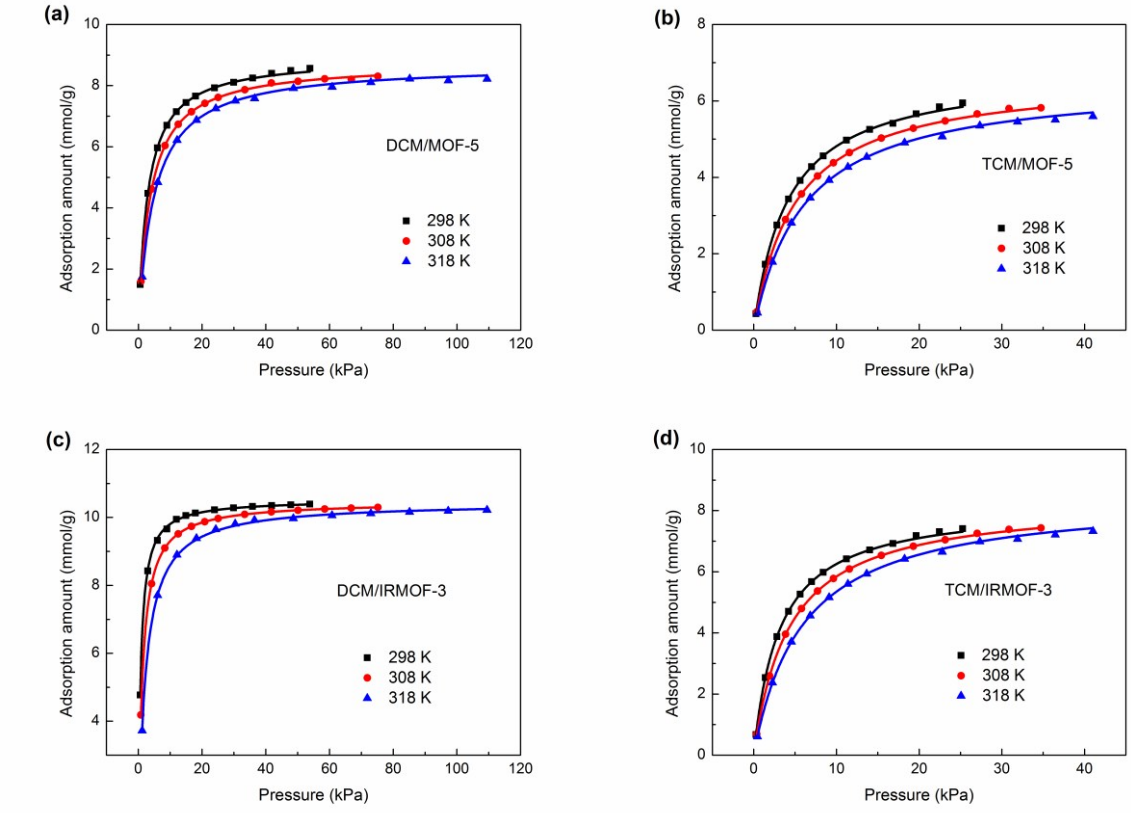

Fig.4 Adsorption isotherms of (a) DCM on MOF-5; (b) TCM on MOF-5; (c) DCM on IRMOF-3; (d) TCM on IRMOF-3 and the fittings of Langmuir equation at 298-318 K. The symbols are the experimental values; the lines are the fits with Langmuir isotherm.

on these two adsorbents was mainly physical. To further study the adsorption behavior of DCM and TCM on the MOF-5 and IRMOF-3, the Langmuir equation was applied to fit the experimental isotherm data. The Langmuir isotherm is written as

$$q = \frac{a_m bp}{1+bp} \qquad (1)$$

Where q (mmol/g) is the adsorbed amount; p is the pressure (kPa); a_m (mmol/g) is the monolayer adsorption capacity; b (kPa^{-1}) is the Langmuir adsorption affinity constant.

Fig. 4 exhibits the comparisons of the experimental equilibrium adsorption data and the isotherm equation fits. It is visible that the Langmuir equation give a better fit to the experimental equilibrium adsorption data of DCM and TCM. Table 2 gives the fitting parameters of the Langmuir isotherm as well as their linear correlation coefficients (R^2) representing coincidence degree between the experimental data and the isotherm equation fits. The data in Table 2 indicates that the linear correlation coefficients (R^2) of the both isotherm equations fit are all above 0.99. It demonstrates that the Langmuir model can well describe the adsorption behavior of DCM and TCM on the MOF-5 and IRMOF-3. As shown in Table 2, the value of b also depicts a downtrend as the temperature increase. It is indicated that adsorption interaction of the MOFs towards DCM and TCM becomes weaker as the temperature increases.[34] Meanwhile, the adsorption capacity of DCM and TCM on the MOF-5 is slightly decreased with temperature increasing, including a physisorption-type interaction.[35]

The strength of the affinity between the adsorbate and the adsorbent surface can be given by the values of Henry constants. In the Henry's law region, i.e. at low pressures, the interactions between the adsorbed molecules are negligible. In the Henry's law region the adsorption loading is directly proportional to the pressure:

$$q = K_H p \qquad (2)$$

where the coefficient K_H (extracted from the slope of the isotherm in the low pressure region) is known as Henry's law constant. The product of the two Langmuir constants (a_m and b) generates the Henry's constant (K_H). As shown in Table 2, the Henry's constants decrease with increasing temperature, as expected, reflecting the decrease of adsorbate-adsorbent affinity with temperature. DCM possesses the larger Henry's constants than TCM at the three temperatures, revealing its strongest interaction with the MOF due to its larger dipole moment compared with TCM.

The selectivity of DCM/TCM mixtures in MOF-5 and IRMOF-3 was also estimated using IAST based on the pure adsorption Langmuir model fitting parameters. Assuming an equilibrium based separation, the adsorbents can be chosen by the separation factor, $\alpha_{1/2}$. Thus, this separation factor, also known as ideal selectivity, represents the affinity of the adsorbent for a species1 over a species 2 and can be calculated by the following equation:

$$\alpha_{1/2} = \frac{K_{H1}}{K_{H2}} \qquad (3)$$

Adsorption selectivity in a binary be defined as:

$$S_{ads,1/2} = \alpha_{1/2} \frac{y_2}{y_1} \qquad (4)$$

where y_1 and y_2 denote the molar fractions of component 1 and component 2 in the gas phase, respectively. Ideal selectivities $\alpha_{1/2}$ of the MOF-5 and IRMOF-3 were calculated based on the Henry's law constants of DCM and TCM. Adsorption selectivity of DCM/TCM on the MOF-5 and IRMOF-3 predicted by IAST for equimolar mixtures (1:1) of DCM/TCM vapor at 298 K, 308 K, and 318 K. The selectivity of DCM/TCM decreases with increasing temperature at the same pressure. The $S_{ads,\ DCM/TCM}$ of MOF-5 are appropriately 1.83, 1.76, and 1.66 at 298 K, 308 K and 318 K, respectively. In comparison, the $S_{ads,\ DCM/TCM}$ of IRMOF-3 are appropriately 5.62, 4.29, and 3.28 at 298 K, 308 K and 318 K, respectively. At the same temperature and pressure, IRMOF-3 showed higher adsorption selectivity than MOF-5.

3.3 Isosteric Heat of Adsorption

Isosteric heat of adsorption is also an important parameter to evaluate the interaction between the adsorbate molecules and the adsorbent surface through physical adsorption. The isosteric heat of adsorption at a given amount can be calculated by the Clausius-Clapeyron equation as

$$Q_{st} = -RT^2 \left(\frac{\partial \ln P}{\partial T} \right)_a \qquad (5)$$

where Q_{st} is the isosteric heat of adsorption ($kJ \cdot mol^{-1}$); T is temperature (K); P is pressure (kPa); a is the adsorption amount ($mmol \cdot g^{-1}$); and R is the universal gas constant. Integration of Eq. (5) gives

$$\ln P = \frac{Q_{st}}{RT} + C \qquad (6)$$

where C is an integration constant.

Table 2. Equation Constants for the Langmuir Isotherm Model for all adsorption isotherms

Adsorbents	T/K	DCM			TCM			$\alpha_{D/T}$
		a_m(mmol/g)	b (kPa^{-1})	K_H	a_m(mmol/g)	b(kPa^{-1})	K_H	
MOF-5	298	8.922	0.337	3.007	6.802	0.242	1.646	1.83
	308	8.748	0.267	2.336	6.662	0.199	1.326	1.76
	318	8.701	0.206	1.792	6.540	0.165	1.079	1.66
IRMOF-3	298	10.425	1.410	14.699	8.219	0.318	2.614	5.62
	308	10.467	0.797	8.342	8.351	0.233	1.946	4.29
	318	10.529	0.450	4.738	8.492	0.170	1.444	3.28

In the present study, DCM and TCM adsorption isotherms on MOF-5 and IRMOF-3 at 298, 308, and 318 K were used to make the heat of adsorption plots. The measurement points were achieved by employing the Langmuir model fitting equation. The adsorption isotherms were first converted to adsorption isosteres, a plot of ln *P* versus 1/*T* at a given adsorption amount (see ESI, Fig. S1†). The heat of adsorption was then calculated from the slopes of the isosteres according to Eq. (6). Fig. 5 shows the isosteric heat of DCM and TCM adsorption on the MOF-5 and IRMOF-3 as a function of the adsorption amount. For IRMOF-3, the isosteric heat on both DCM and TCM decreases with loading, indicating the energetic heterogeneity for Cl-VOCs. This heterogeneity is attributed to the interaction between the dipole moment of Cl-VOCs with amino groups. At low surface coverage, molecules are preferably adsorbed onto the amino group sites, whereas at high loading, these sites become saturated and the adsorbate-adsorbent interaction is mainly dispersion. For MOF-5, the isosteric heat on both DCM and TCM slightly increases. While, in the case of MOF-5 the increase in Q_{st} may be attributed to the intersorbate interactions that are promoted in the restricted pore space. The initial Q_{st} of DCM for IRMOF-3 has a value of 44.25 kJ/mol. The high Q_{st} is believed to arise from a combination of DCM-NH_2 interactions. In contrast, the initial Q_{st} of DCM on MOF-5 is 20.61 kJ/mol, 53.4 % lower than that for IRMOF-3. In addition, the initial Q_{st} of TCM on IRMOF-3 (23.26 kJ/mol) is also higher than that on MOF-5 (16.76 kJ/mol). The amino group enhanced isosteric heat of DCM and TCM adsorption on the IRMOF-3. These values confirm the stronger interactions between DCM and TCM and IRMOF-3 as observed in the adsorption isotherms.

3.4 Adsorption Kinetics

Adsorption kinetics and diffusion coefficient are very important parameters for evaluating an adsorbent and designing an adsorption process. Therefore, adsorption kinetics data of DCM and TCM on MOF-5 and IRMOF-3 were collected at the same time when the adsorption equilibrium data were measured. Fig. 6 shows the fractional uptake curves of DCM and TCM on the MOF-5 and IRMOF-3 at a pressure of 2.8 kPa and different temperatures (298, 308, and 318 K). As plotted in Fig. 6, DCM diffuses much faster than TCM on two adsorbents due to the smaller molecule size (with a kinetic diameter of 3.3 Å against 6.5 Å of TCM). It was observed that the kinetic curve of both DCM and TCM adsorption on the MOF-5 were steeper than those of adsorption on the IRMOF-3. For MOF-5, it took 41.7 min for DCM and 106.8 min for TCM to reach equilibrium, whereas for the IRMOF-3, it took 66.9 min for DCM and 238.9 min for TCM to reach the equilibrium point at 298 K and 2.8 kPa (see ESI, Fig. S2†). This indicates that the adsorption rates of both Cl-VOCs on the MOF-5 were higher than those on IRMOF-3, which was mostly due to its larger pore size compared with the IRMOF-3. In addition, it can be seen that for both DCM and TCM when the higher adsorption temperature was applied, a slightly shorter time was required for the equilibrium to arrive.

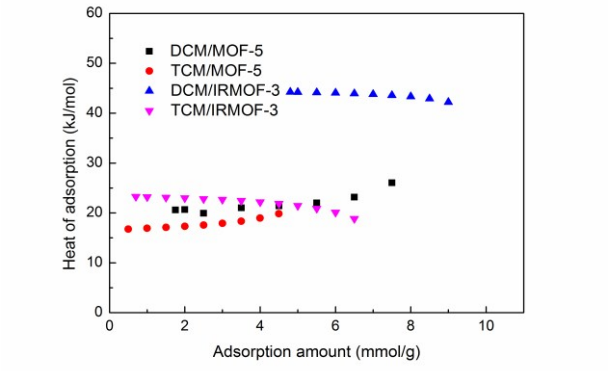

Fig.5 Dependence of isosteric adsorption heat on the amounts adsorbed of DCM and TCM on the MOF-5 and IRMOF-3

A classical micropore diffusion model[36] was applied to correlate the adsorption kinetics data and extract the intracrystalline diffusivity for DCM and TCM in MOF-5 and IRMOF-3. By neglecting the heat transfer between particle and surrounding fluid, the diffusion equation in a spherical coordinate is written as:

$$\frac{\partial q}{\partial t}=\frac{1}{r^2}\frac{\partial}{\partial r}\left(r^2 D_c \frac{\partial q}{\partial r}\right) \quad (7)$$

where r is the radius of the equivalent sphere, D_c is the intracrystalline diffusivity and $q(r, t)$ is adsorbed amount at time t and radial position r. For constant diffusivity for a particular pressure, Eq. 7 can be converted to

$$\frac{\partial q}{\partial t}=D_c\left(\frac{\partial^2 q}{\partial r^2}+\frac{2}{r}\frac{\partial q}{\partial r}\right) \quad (8)$$

The solution for the equivalent radius r_c is given by

$$\frac{\bar{q}-q_0'}{q_0-q_0'}=\frac{m_t}{m_\infty}=1-\frac{6}{\pi^2}\sum_{n=1}^{\infty}\frac{1}{n^2}\exp\left(\frac{-\pi^2 D_c t}{r_c^2}\right) \quad (9)$$

where $\bar{q}$ is the average adsorbate amount in the particle, q_0' is the initial adsorption amount in the particle, q_0 is the equilibrium uptake in the particle, and m_t/m_∞ is the fractional adsorption uptake. $\bar{q}$ was given by

$$\bar{q}=\frac{3}{r_c^3}\int_0^{r_c} q r^2 dr \quad (10)$$

The fractional adsorption uptake (m_t/m_∞) can be correlated with the diffusion time constant by the following equation if the fractional adsorption uptake is greater than 70%.

$$1-\frac{m_t}{m_\infty}=\frac{6}{\pi^2}\exp\left(\frac{-\pi^2 D_c t}{r_c^2}\right) \quad (11)$$

The diffusion time constant (D_c/r_c^2, s^{-1}) were calculated from the slope of a linear plot of $\ln(1-(m_t/m_\infty))$ greater than 70% and less than 99% were used for estimating the diffusion time constants. The intracrystalline diffusion coefficient (D_c, cm^2/s) was calculated from the diffusion time constant. The crystallite radius, r_c, for MOF-5 (r_c=1.5·10^{-5} m) and IRMOF-3 (r_c=1.75·10^{-5} m) were estimated from their SEM images.

The plots of fractional DCM and TCM adsorption uptakes on MOF-5 and IRMOF-3 against the adsorption time at different temperatures (298, 308, and 318 K) with the same pressure 2.8 kPa were showed in ESI Fig. S3†. It can be seen from Fig. S3 that the fits of the three groups of experiment data are very

high linearity (with correlation coefficients R^2 of more than 0.99), suggesting that DCM and TCM diffusion within the MOF can be well described by Eq. (11). From the slopes of these fitting straight lines shown by Fig. S3, the diffusion time constants and diffusion coefficients of DCM and TCM within the MOF-5 and IRMOF-3 are obtained, as listed in Table 3. The ratio of diffusion time constant of DCM and TCM gives the DCM/TCM kinetic selectivity. It can be seen that the diffusivity of DCM on both adsorbents is higher than that of TCM. This is because the kinetic diameter of DCM is 3.3 Å, which is smaller than the kinetic diameter of TCM (6.5 Å). We hypothesized that the slightly smaller molecule size of DCM might have facilitated the diffusion. In addition, the lower diffusivity of both gases at corresponding temperatures was observed on the IRMOF-3, which could be contributed to the smaller pore size and pore volume compared to the MOF-5. Considering the average particle radius r_c of the MOF-5 (~15 μm), the diffusivities of DCM and TCM were estimated to be in the order of 2.25-2.75×10^{-8} cm^2/s and 0.88-1.22×10^{-8} cm^2/s, respectively. Since the average particle radius r_c of the IRMOF-3 samples is 17.5 μm, the diffusion coefficients (D_c) of DCM and TCM on the IRMOF-3 at 298-318 K can be found to be in range of 1.92-2.82×10^{-8} cm^2/s and 0.49-0.99×10^{-8} cm^2/s, respectively. The diffusion time constant for DCM and TCM in MOF-5 are estimated to be 1.03×10^{-2} and 0.39×10^{-2} s^{-1} at 298 K, suggesting a modest kinetic selectivity of 2.64 for DCM/TCM separation. In comparison, the diffusion time constant for DCM and TCM in IRMOF-3 are estimated to be 0.62×10^{-2} and 0.16×10^{-2} s^{-1} at 298 K, suggesting a higher kinetic selectivity of 3.88 than that of MOF-5 for DCM/TCM separation. In addition, Table 3 indicates that both the diffusion time constants and the diffusion coefficients increased with temperature, which indicates that the diffusion rate can be enhanced by increasing the temperature properly.

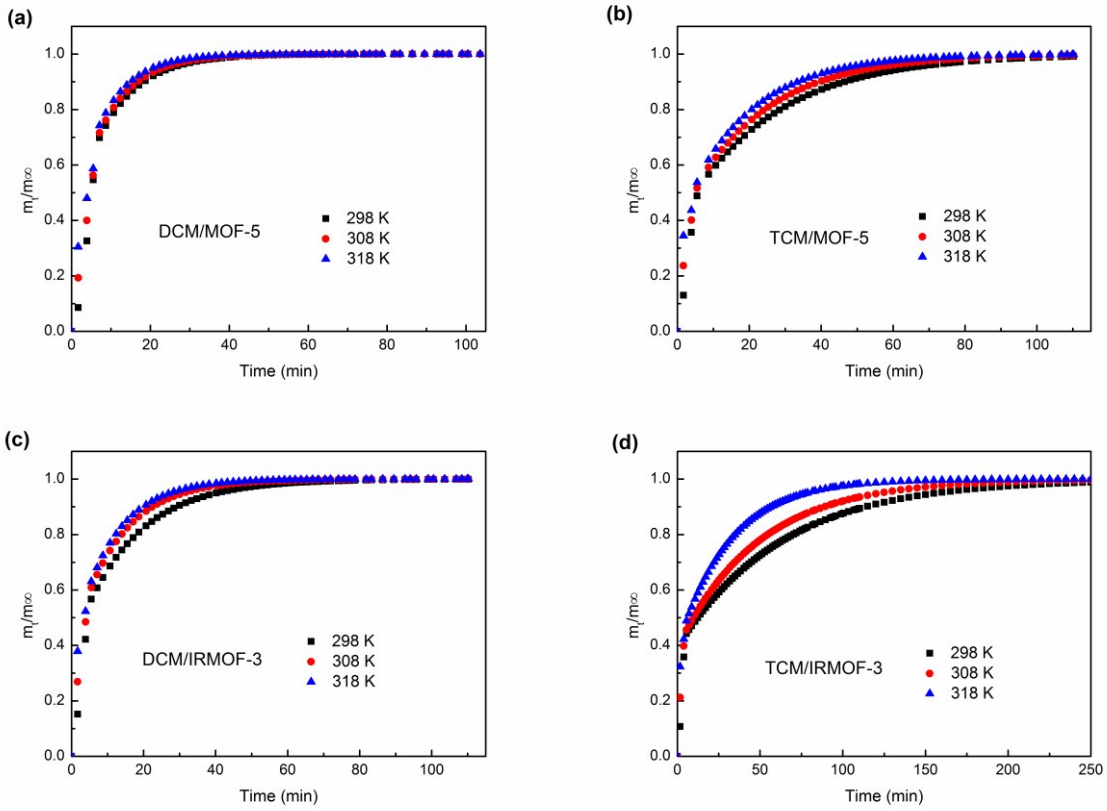

Fig.6 Fractional DCM adsorption uptakes on the MOF-5 (a) and IRMOF-3 (c) and fractional TCM adsorption uptakes on the MOF-5 (b) and IRMOF-3 (d) at different temperatures (298, 308, 318 K) and 2.8 kPa.

Table 3. DCM and TCM diffusion time constants and diffusion coefficient within the MOF-5 and IRMOF-3 measured in this work

Adsorbents	T/K	DCM D_c/r_c^2 (10^{-2} s^{-1})	DCM D_c (10^{-8} cm^2/s)	TCM D_c/r_c^2 (10^{-2} s^{-1})	TCM D_c (10^{-8} cm^2/s)	DCM/TCM kinetic selectivity
MOF-5	298	1.03	2.25	0.39	0.88	2.64
	308	1.09	2.45	0.46	1.04	2.37
	318	1.22	2.75	0.54	1.22	2.26
IRMOF-3	298	0.62	1.92	0.16	0.49	3.88
	308	0.81	2.49	0.23	0.72	3.52
	318	0.92	2.82	0.32	0.99	2.85

Diffusion selectivity can be defined as[37]:

$$S_{diff,1/2} = D_{1,self} / D_{2,self} \quad (12)$$

Where $D_{1,\text{self}}$ and $D_{2,\text{self}}$ are the self-diffusivity of species 1 and 2, respectively (m^2/s). Therefore, the $S_{\text{diff, DCM/TCM}}$ of MOF-5 are appropriately 2.64, 2.37, and 2.26 at 298 K, 308 K and 318 K, respectively. In comparison, the $S_{\text{diff, DCM/TCM}}$ of IRMOF-3 are appropriately 3.88, 3.52, and 2.85 at 298 K, 308 K and 318 K, respectively.

For membrane processes the permeation selectivity, $S_{\text{perm, 1/2}}$ can be expressed as follows:

$$S_{perm,1/2} = S_{ads,1/2} \times S_{diff,1/2} \quad (13)$$

Then from Eq. (13), we can get the permeation selectivity of DCM over TCM vapor on the MOF-5 membrane of about 4.83 by using $S_{\text{ads, DCM/TCM}}$ of 1.83 and $S_{\text{diff, DCM/TCM}}$ of 2.64 under very similar conditions (298 K and 2.8 kPa). The permeation selectivity of DCM over TCM vapor on the IRMOF-3 membrane of about 21.81 by using $S_{\text{ads, DCM/TCM}}$ of 5.62 and $S_{\text{diff, DCM/TCM}}$ of 3.88 under very similar conditions (298 K and 2.8 kPa). Clearly, the selectivity of DCM/TCM vapor in the membrane-assisted separation process will be much higher than that in the adsorption process due to the discrepancy of adsorption and diffusion behavior between DCM and TCM vapor in the IRMOF-3.

3.5 Adsorption activation energy

The Arrhenius equation can usually be applied to estimate adsorption/diffusion activation energy of an adsorbate on an adsorbent. According to the Arrhenius equation, the relationship between the diffusion coefficient (D_c) of the adsorbate and the activation energy (E_a) for adsorption within the MOF-5 or IRMOF-3 is represented by following equation:

$$D_c = A\exp\left(\frac{-E_a}{RT}\right) \quad (14)$$

where D_c is diffusion coefficient, A is a constant, E_a is the adsorption activation energy, kJ/mol, R is the universal gas constant, and T is the temperature, K. Eq. (14) can be transformed into a linear equation:

$$\ln D_c = \ln A - \frac{E_a}{RT} \quad (15)$$

Then, the Arrhenius plot of ln D_c versus 1/T can be obtained on the basis of Eq. (15), as shown in Fig. 7. The adsorption activation energy E_a of DCM and TCM on the MOF-5 and IRMOF-3 can be calculated from the slope of the fitting line in Fig. 7. The activation energy E_a for DCM diffusion in MOF-5 and IRMOF-3 is found to be 7.9 and 15.2 kJ/mol, respectively. The activation energy E_a for TCM diffusion in MOF-5 and IRMOF-3 is found to be 12.7 and 27.5 kJ/mol, respectively. The adsorption activation energy for TCM is higher than that of DCM on both MOF-5 and IRMOF-3, suggesting DCM molecules can adsorbed on the MOFs much easier than TCM molecules.

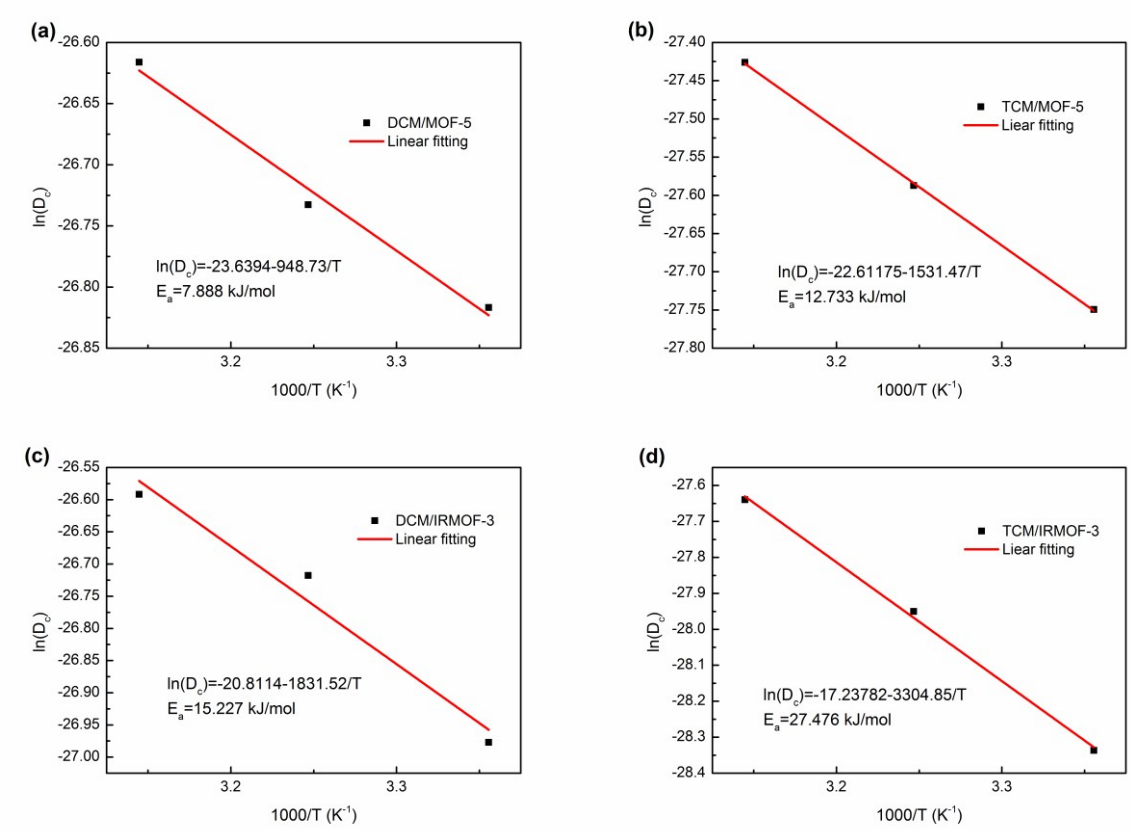

Fig.7 Arrhenius plot of DCM diffusivity in the MOF-5 (a) and IRMOF-3 (c) and Arrhenius plot of TCM diffusivity in the MOF-5 (b) and IRMOF-3 (d).

4. Conclusions

In conclusion, MOF-5 and IRMOF-3 were prepared and investigated systematically of their adsorption and separation property of DCM and TCM. The Langmuir model was used to model the experimental adsorption data. In spite of the reduced porosity of IRMOF-3, the adsorption capacity of DCM and TCM were improved up to 24.5 % and 27.4 % when compared with MOF-5. The isosteric heat of DCM and TCM adsorption on IRMOF-3 were much higher than those on MOF-5 due to the stronger interaction between Cl-VOCs molecules and the amino group on IRMOF-3. The diffusion time constants of DCM in the MOF-5 and IRMOF-3 were estimated to be 2.25×10^{-8} cm²/s and 0.88×10^{-8} cm²/s at 298 K, respectively. The diffusion time constants of TCM in the MOF-5 and IRMOF-3 were estimated to be 1.92×10^{-8} cm²/s and 0.49×10^{-8} cm²/s at 298 K, respectively. Furthermore, the adsorption selectivity and diffusion selectivity of DCM/TCM on the IRMOF-3 was of about 5.62 and 3.88 at 298 K and 2.8 kPa, which are higher than those of MOF-5. The improved adsorption capacity and enhanced adsorption selectivity and diffusion selectivity over IRMOF-3 (with amino group) could be attributed to the improved interaction of Cl-VOCs with the amino group on MOFs. This work may form the basis for design adsorbents with particular pore size, pore shape, and chemical functionality resulting for significant advances in the fields of gas adsorption and separation.

Acknowledgements

This work was supported by the National Natural Science Foundation of China No. 21376026.

References

1 H. Furukawa, N. Ko, Y. B. Go, N. Aratani, S. B. Choi, E. Choi, A. O. Yazaydin, R. Q. Snurr, M. O'Keeffe, J. Kim and O. M. Yaghi, *Science*, 2010, **329**, 424-428.
2 Z. Zhang, Y. Chen, X. Xu, J. Zhang, G. Xiang, W. He and X. Wang, *Angew. Chem. Int. Edit.*, 2014, **53**, 429-433.
3 K. Sumida, D. L. Rogow, J. A. Mason, T. M. McDonald, E. D. Bloch, Z. R. Herm, T. Bae and J. R. Long, *Chem. Rev.*, 2012, **112**, 724-781.
4 S. Noro, S. Kitagawa, T. Akutagawa and T. Nakamura, *Prog. Polym. Sci.*, 2009, **34**, 240-279.
5 Y. H. Hu and L. Zhang, *Adv. Mater.*, 2010, **22**, E117-E130.
6 W. Gao, Y. Chen, Y. Niu, K. Williams, L. Cash, P. J. Perez, L. Wojtas, J. Cai, Y. Chen and S. Ma, *Angew. Chem. Int. Edit.*, 2014, **53**, 2615-2619.
7 K. Sumida, D. L. Rogow, J. A. Mason, T. M. McDonald, E. D. Bloch, Z. R. Herm, T. Bae and J. R. Long, *Chem. Rev.*, 2012, **112**, 724-781.
8 J. Li, J. Sculley and H. Zhou, *Chem. Rev.*, 2012, **112**, 869-932.
9 A. Corma, H. Garcia and F. X. L. I. Llabres I Xamena, *Chem. Rev.*, 2010, **110**, 4606-4655.
10 M. Zhao, K. Deng, L. He, Y. Liu, G. Li, H. Zhao and Z. Tang, *J. Am. Chem. Soc.*, 2014, **136**, 1738-1741.
11 L. He, Y. Liu, J. Liu, Y. Xiong, J. Zheng, Y. Liu and Z. Tang, *Angewandte Chemie International Edition*, 2013, **52**, 3741-3745.
12 R. Babarao, C. J. Coghlan, D. Rankine, W. M. Bloch, G. K. Gransbury, H. Sato, S. Kitagawa, C. J. Sumby, M. R. Hill and C. J. Doonan, *Chem. Commun.*, 2014, **50**, 3238-3241.
13 B. Seoane, C. Téllez, J. Coronas and C. Staudt, *Sep. Purif. Technol.*, 2013, **111**, 72-81.
14 S. Kim, J. Kim, H. Kim, H. Cho and W. Ahn, *Catal. Today*, 2013, **204**, 85-93.
15 N. Wang, A. Mundstock, Y. Liu, A. Huang and J. Caro, *Chem. Eng. Sci.*, 2015, **124**, 27-36.
16 I. Ahmed and S. H. Jhung, *J. Hazard. Mater.*, 2015, **283**, 544-550.
17 S. Rostamnia, H. Xin and N. Nouruzi, *Micropor. Mesopor. Mat.*, 2013, **179**, 99-103.
18 Y. Kim and D. Park, *J. Nanosci. Nanotechno.*, 2013, **13**, 2307-2312.
19 F. X. Llabres I Xamena, F. G. Cirujano and A. Corma, *Micropor. Mesopor. Mat.*, 2012, **157**, 112-117.
20 N. T. S. Phan, T. T. Nguyen, Q. H. Luu and L. T. L. Nguyen, *Journal of Molecular Catalysis A: Chemical*, 2012, **363-364**, 178-185.
21 X. Wang, H. Fan, Z. Tian, E. He, Y. Li and J. Shangguan, *Appl. Surf. Sci.*, 2014, **289**, 107-113.
22 B. Huang, C. Lei, C. Wei and G. Zeng, *Environ. Int.*, 2014, **71**, 118-138.
23 F. Tian, X. Zhang and Y. Chen, *RSC Advances*, 2016, **6**, 31214-31224.
24 Z. Zhao, Z. Li and Y. S. Lin, *Ind. Eng. Chem. Res.*, 2009, **48**, 10015-10020.
25 X. Wang, H. Fan, Z. Tian, E. He, Y. Li and J. Shangguan, *Appl. Surf. Sci.*, 2014, **289**, 107-113.
26 C. McKinstry, E. Cussen, A. Fletcher, S. Patwardhan and J. Sefcik, *Cryst. Growth Des.*, 2013, **13**, 5481-5486.
27 D. Saha and S. Deng, *J. Colloid Interf. Sci.*, 2010, **348**, 615-620.
28 X. Wang, H. Fan, Z. Tian, E. He, Y. Li and S. Ju, *Appl. Surf. Sci.*, 2014, **289**, 107-113.
29 D. Kim, T. B. Lee, S. B. Choi, J. H. Yoon, J. Kim and S. Choi, *Chem. Phys. Lett.*, 2006, **420**, 256-260.
30 S. Hsu, C. Huang, T. Chung and S. Gao, *Journal of the Taiwan Institute of Chemical Engineers*, 2014, **45**, 2526-2530.
31 B. T. Clausse, B. Garrot, C. Cornier, C. Paulin, M. Simonot-Grange and F. Boutros, *Micropor. Mesopor. Mat.*, 1998, **25**, 169-177.
32 W. G. Shim, J. W. Lee and H. Moon, *Journal of Chemical & Engineering Data*, 2003, **48**, 286-290.
33 T. Kawai, T. Yanagihara and K. Tsutsumi, *Colloid Polym. Sci.*, 1994, **272**, 1620-1626.
34 A. R. Zimmerman, K. W. Goyne, J. Chorover, S. Komarneni and S. L. Brantley, *Org. Geochem.*, 2004, **35**, 355-375.
35 F. Xu, S. Xian, Q. Xia, Y. Li and Z. Li, *Adsorpt. Sci. Technol.*, 2013, **31**, 325-339.
36 W. Kast, *Chemical Engineering and Processing: Process Intensification*, 1985, **19**, 118.
37 R. Krishna and J. M. van Baten, *J. Membrane Sci.*, 2011, **369**, 545-549.

One sentence for graphical abstract:

MOF functionalized with $-NH_2$ exhibits improved adsorption capacity and selectivity for adsorption and separation of dichloromethane and trichloromethane.

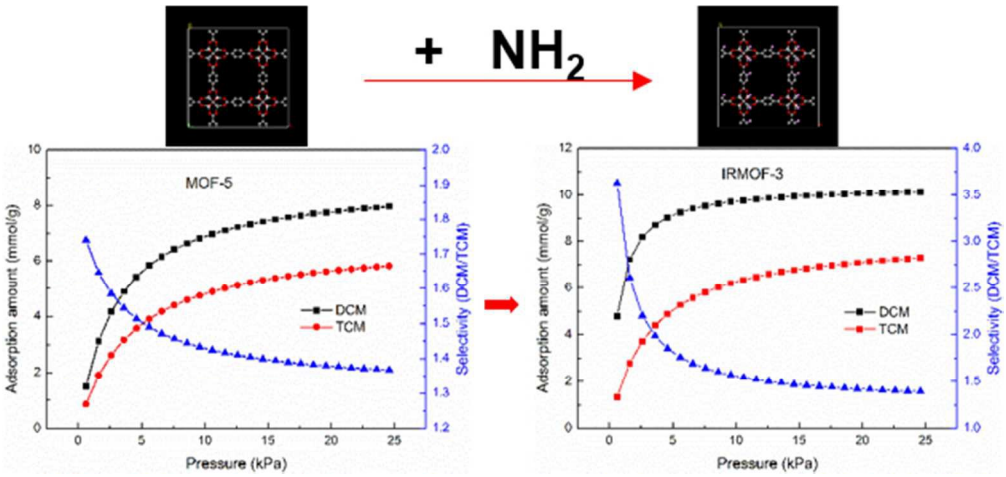

166x78mm (96 x 96 DPI)